Research paper

Synthesis, characterization and properties of a new nitrogen-rich ANQ-based salt : 1-amino-2-nitroguanidinium 3,5-dinitro-1,2,4-triazole

Xinghui Jin*†, Jianhua Zhou*, Bingcheng Hu**, and Ling Wang*

*School of Chemistry and Pharmaceutical Engineering, Qilu University of Technology, Ji'nan 250353, CHINA
  Phone: +86 0531−89631028
†Corresponding author: jingetiema0000@126.com

**School of Chemical Engineering, Nanjing University of Science and Technology, Nanjing, 210094, CHINA

Abstract

A new nitrogen-rich ANQ-based energetic material 1-amino-2-nitroguanidinium 3,5-dinitro-1,2,4-triazole salt was synthesized and its chemical and physical properties were fully investigated. TG-DSC curves show that the thermal decomposition process of the title compound can be divided in to 4 stages and the third stage is the main procedure which shows a sharp exothermic peak at about 217.1 °C with a measured decomposition enthalpy of 1252 J g^{-1}. Additionally, the calculated critical temperature of thermal explosion (411.1K) was also calculated. In view of the electronic density, energy gap between HOMO and LUMO (0.16311 a.u.) and electrostatic potential (ESP) on molecular surface, it is predicted that the title salt has a stable structure according to the stability criterion. Additionally, the title salt possesses high heat of formation (ΔH_f, 354.7 kJ mol^{-1}) and moderate detonation properties (D, 8.4 km s^{-1}; P, 29.8 GPa), suggesting that the title salt can be considered as a potential candidate of energetic materials.

Keywords: energetic salt, 1-amino-2-nitroguanidinium 3,5-dinitro-1,2,4-triazole, thermal behavior, electron structure, energetic properties

1. Introduction

Nitrogen-rich compounds, especially nitrogen-rich salts have gained much attention due to their high positive heat of formation, excellent detonation properties and environmental friendliness[1]−[4]. However, it is found that there appears sharp contradictions regarding to the excellent detonation properties and stabilities[5]. Previous research show that amino groups can improve the stability of a compound while nitro group will decrease the stability of a compound though it can improve the density and detonation properties[6]−[8]. And therefore, the protonated 1-amino-2-nitroguanidine (ANQ), in which exits both amino and nitro groups, was selected as the energetic cation[9],[10]. On the other hand, azoles (such as diazole, triazole and tetrazole) usually contain a large number of inherently energetic C−N and N−N bonds and will help improve the heat of formation during the decomposition process[11]. It is also reported that thermal decomposition point of 3,5-dinitro-1,2,4-triazole is the best compared with 2,4,5-trinitroimidazole and 5-nitrotetrazole[12] (Figure 1). Thus, the deprotonated 3,5-dinitro-1,2,4-triazole was selected as the energetic anion in order to improve the detonation properties and thermal stabilities.

In this study, a new nitrogen-rich energetic material 1-amino-2-nitroguanidinium 3,5-dinitro-1,2,4-triazole salt was synthesized (Figure 2, compound 3) and characterized. Its thermal decomposition process, thermal dynamic parameters, natural bond orbital (NBO) charges, frontier
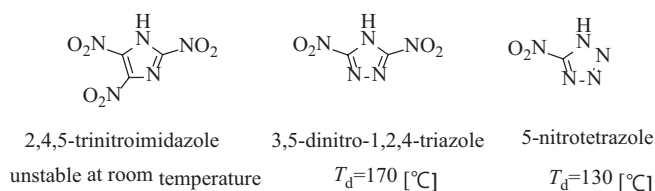

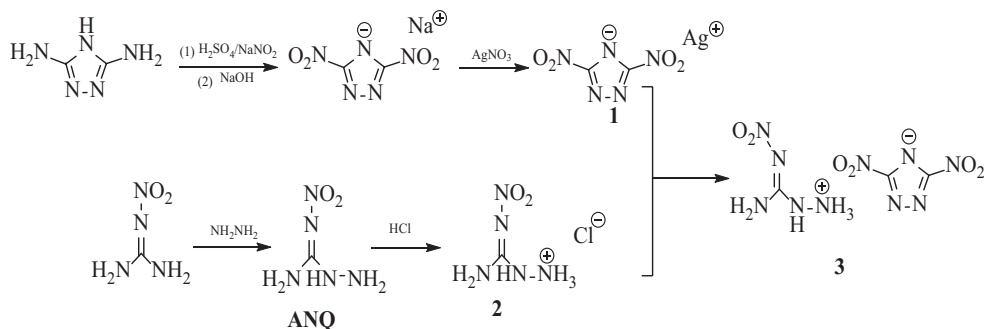Figure 1   Thermal stability of C-nitrated azoles.

Figure 2   Synthesis of 1-amino-2-nitroguanidinium 3,5-dinitro-1,2,4-triazole (compound 3).

molecular orbital (FMO), electrostatic potential (ESP) and detonation properties were also investigated to give a better understanding of its physical and chemical properties.

2. Experimental
2.1 Synthesis

Sliver 3,5-dinitro-1,2,4-triazole salt (compound 1) was synthesized according to the literature[13].

Synthesis of 1-amino-2-nitroguanidinium chloride (compound 2): To a vigorous stirred solution of concentrated hydrochloric acid was added ANQ (1.19 g, 10 mmol) partially and the suspension was heated until all the ANQ were dissolved. Then the transparent liquid reacted at 80 °C for 2 h. Cool down to the room temperature and 1-amino-2-nitroguanidinium chloride were precipitated as white needle crystal.

Yield: 1.12 g, 71.9%; IR (KBr), ν (cm^{-1}): 3333, 3129, 3002, 1635, 1585, 1484, 1340, 1275, 1225, 1198, 906, 665, 485; ^{1}H NMR (500 MHz, DMSO-d_6) δ: 6.53 (s, 3H), 8.36 (s, 2H) 9.75 (s, 1H); ^{13}C NMR (125 MHz, DMSO-d_6) δ: 161.27; ESI-MS (m/z): 120 [M+H]$^+$.

Synthesis of 1-amino-2-nitroguanidinium 3,5-dinitro-1,2,4-triazole salt (compound 3): To a vigorous stirred suspension of silver 3,5-dinitro-1,2,4-triazole salt (2.66 g, 10 mmol) was added the solution of 1-amino-2-nitroguanidinum chloride (1.55 g, 10 mmol) slowly. The resulting suspension was stirred at 40 °C for 6 h and then filtered. The filtrate was concentrated and the collected residue was re-crystallized from methanol/water to afford the colorless 1-amino-2-nitroguanidinium 3,5-dinitro-1,2,4-triazole salt.

Yield: 2.47 g, 89.0%; IR (KBr), ν (cm^{-1}): 3340, 3308, 3217, 2158, 1635, 1554, 1498, 1393, 1358, 1283, 1179, 1109, 1025, 916, 864, 706, 651; ^{1}H NMR (500 MHz, DMSO-d_6,) δ: 6.69 (s, 5H), 8.38 (s, 1H); ^{13}C NMR (125 MHz, DMSO-d_6) δ: 159.45, 163.22; ESI-MS (m/z): 158 [M-H]$^-$, 120 [M+H]$^+$.

2.2 Theoretical studies

All the quantum chemical calculations were performed on the Gaussian 03 suite of programs[14] using B3LYP functional with 6-31+G (d, p) basis set of density functional theory. All of the optimized structures were characterized to be true local energy minima on the potential energy surface without imaginary frequencies.

3. Results and discussion
3.1 Thermal behavior

Thermal decomposition process of compound 3 was performed on a NETZSCH STA 409 PC/PG instrument with about 2.44 mg sample placed in alumina crucibles under the nitrogen atmosphere (flow rate: 35 ml min^{-1}). TG-DTG-DSC curves that recorded under the heating rate of 5 K min^{-1} from 35 °C up to 500 °C were shown in Figure 3. From TG curve in the figure, it is seen that the thermal decomposition behavior of compound 3 is a 4 stage process: (1) The first step is an endothermic reaction with about 5% weight loss which may be caused by the loss of crystal water; (2) The second step and the third step, which starts from 100 to 130°C and starts from 130 to 180°C with a mass loss of 17% respectively, may due to the loss of nitro group; (3) The fourth step, which starts from 180 to 230 °C with a mass loss of 35%, may be caused by the decomposition of the triazole ring. Correspondingly, 3 evident sharp peaks and 1 weak peak were also found in the DTG curve which demonstrated the fact that the pyrolysis process of compound 3 can be divided into 4 stages. Furthermore, a sharp exothermic peak was also found in DSC curve at about 217.1 °C with a measured decomposition enthalpy of 1252 J g^{-1}.

3.2 Non-isothermal decomposition kinetics and thermal safety

In order to give a full investigation on the thermal behavior of compound 3, TG-DSC curves of at different heating rates of 5, 10, 15 and 20 K·min^{-1} were recorded in Figure 4. As a result of the "thermal hysteresis" of the heat
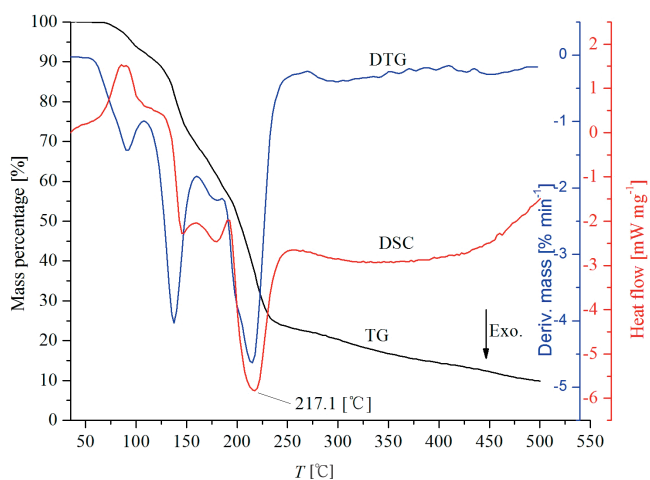

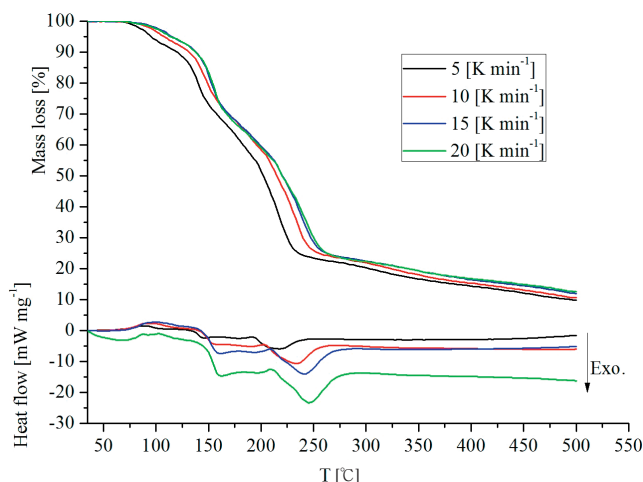**Figure 3**   TG-DTG-DSC curves at the heating rate of 5 K min^{-1}.

Figure 4　TG -DSC curves at different heating rate of 5, 10, 15, 20K min^{-1}.

transfer effect, it is clearly seen from the DSC curves that the exothermic peak temperatures increased as the heating rates increasing[15].

Thermal kinetic values such as pre-exponential constant (A) and activation energy (E) were calculated based on the non-isothermal DSC curves combined with Kissinger and Ozawa's methods. The equations can be written as follows :

Kissinger's method[16] :

$$\ln\left(\beta/T_{pi}^2\right) = \ln\left(A_K \cdot R/E_K\right) - E_K/(R \cdot T_{pi}) \qquad (1)$$

where β stands for the heating rate, T_{pi} stands for maximum peak temperature, R stands for the gas constant. Then, values of A and E_k were calculated by plotting $\ln\left(\beta_i/T_{pi}^2\right)$ vs. reciprocal of the temperature (T^{-1}). Ozawa-Doyle's method[17] :

$$\log\beta = \log(A \cdot E_O)/[R \cdot G(\alpha)] - 2.315 - 0.4567E_o/(R \cdot T_{pi}) \quad (2)$$

where α stands for conversion ratio, E_O stands for apparent activation energy, A stands for the pre-exponential factor, T stands for peak temperature, R stands for gas constant and β stands for heating rate. In order to reduce the computational procedure, a simplified form of Equation (3) were written as follows :

$$\log\beta = const. - 0.4567E_O/(R \cdot T_{pi}) \qquad (3)$$

The critical temperature of thermal explosion (T_b) is also an important parameter to evaluate the thermal stability of an explosive since it is an essential factor to evaluate the safety during storage or process operations. The value can be calculated by the following equations[18] :

$$T_{pi} = T_{p0} + b \cdot \beta_i + c \cdot \beta_i^2 + d \cdot \beta_i^3 \qquad (4)$$

$$T_b = \left(E_o - \sqrt{E_o^2 - 4E_o \cdot R \cdot T_{p0}}\right)/2R \qquad (5)$$

E_o, the apparent activation energy obtained by Ozawa's method ; R, the gas constant ; T_{p0}, the peak temperature corresponding to $\beta \rightarrow 0$.

Then values of E_k, E_o, A, r_k, r_o and T_b of stage 2, 3 and 4 were obtained and summarized in Table 1 because the they are the main decomposition stage of the energetic salt. Obviously, the calculated activation energy of stage 2, 3 and 4 by Kissinger method were similar to those of Ozawa's method which indicate that the results were credible. It is also found that T_b of stage 2, 3 and 4 were 411.1 K, 456.8 K and 461.8 K, respectively.

3.3　NBO charges and electronic density

Natural bond orbital (NBO) charges[19], which can supply useful information on the interactions among bonds, were calculated and presented in Figure 5. It is seen that most of the positive charges were located on the carbon and hydrogen atoms while most of the negative charges were localized on the oxygen and nitrogen atoms. C1 is the most positive compared with C15 and C16, and this may be caused by the electron-withdrawing effect of N-NO$_2$ group that attached to C1 atom combined with the π-conjugated effect that located in the triazole ring. As for the nitrogen atoms, N6 is the most negative while N18 possesses the least negative charges. It also should be note that N3, N20 and N23 atoms that located in nitro group possess positive charges while the other nitrogen atoms posses negative charges which may be caused by strong electron-withdrawing effect of the oxygen atoms located in nitrogen groups. Besides, as a result of π-conjugated effect that located in the triazole ring, N3 (0.61026 e) is more positive than N20 (0.46907 e) and N23 (0.48600 e).

Figure 6 illustrates the contour line map of the electronic density of compound 3 since it is an important
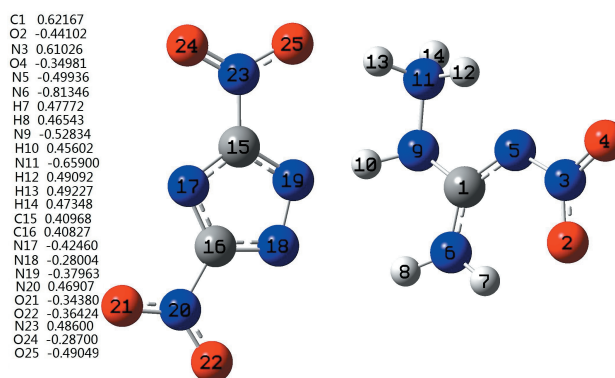

Figure 5　NBO charges distribution on compound 3.

Table 1　Kinetic values of compound 3.

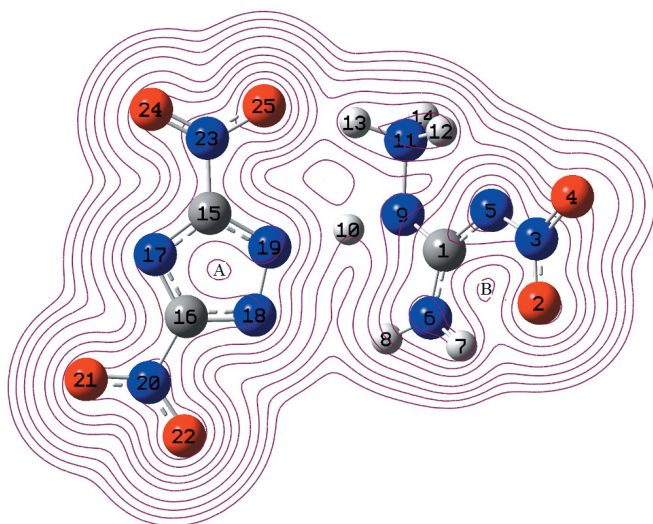| Stage	Kissinger method			Ozawa method			
	E_k[kJ mol^{-1}]	$\log A_k$	r_k	E_o[kJ mol^{-1}]	r_o	T_{p0}[K]	T_b[K]
2	131.6	31.2	0.99	131.9	0.99	400.5	411.1
3	139.2	12.8	0.99	139.7	0.99	444.4	456.8
4	106.4	9.0	0.97	107.3	0.93	445.3	461.8

Figure 6   Contour line map of electronic density of compound 3.

indicator to express the chemical and physical properties of a molecule.It is reported that high peaks correspond to the nuclear charge of the heavy nucleus, which improves electron aggregation and then displays integral exponential attenuation towards all surrounding atoms[20]. As a consequence, electron densities distributed around the oxygen and nitrogen atoms are denser than those distributed around carbon and hydrogen atoms. Additionally, an increasing of electrons was also found around the bonds area (especially on double bonds of the triazole ring) which may be caused by the electron pair sharing between atoms with covalence interaction while delocalization of electronic density was found in the region of A which may improve the stability of anion as well as the compound 3. As for the region of B, the decrease of electronic density may be caused by the following reasons : (1) the repulsive interactions of lone pair electrons among the adjacent atoms (O2 and N6) to decrease the electronic density ; (2) intra-molecular hydrogen bonds between O2 and H7 to form a stable hexatomic ring which may delocalize the electronic density.

3.4 Frontier molecular orbital and density of state

Figure 7 illustrates the 3D plots of the highest occupied molecular orbital (HOMO) and the lowest unoccupied molecularorbital (LUMO) of compound 3 since it can provide much useful information on the electronic structures, chemical reaction and the capability of electron transition from occupied orbitals to unoccupied oribitals[21]. Generally speaking, The smaller the HOMO−LUMO gap in the compound, the easier it would be for the HOMO electrons to cross this gap which results in poor stability. The calculated energy of HOMO, LUMO and their gap of compound 3 were −0.30645 a.u., −0.14334 a.u. and 0.16311 a.u. respectively, suggesting the salt may has a lower reactivity. As for Figure 7, it is obviously found that the HOMO and LUMO levels are distributed mainly on 3,5-dinitro-triazole anion (N atom in -NH group in cation also shows minor contribution to HOMO) and all the orbits are 2-fold degenerate (especially on 3,5-dinitro-triazol ring),
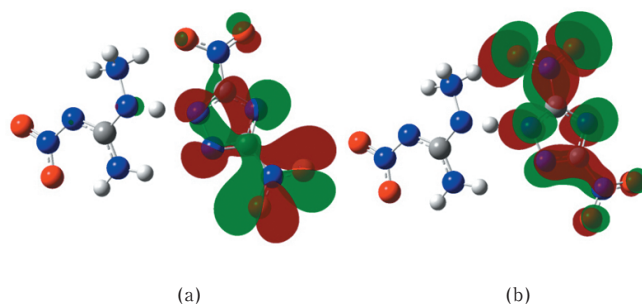

| (a) | (b) |

Figure 7   HOMO (a) and LUMO (b) of compound 3.

indicating that the removal of an electron from the HOMO level or addition of an electron to the LUMO level may be weaken the skeleton framework.

3.5 Electrostatic potential on molecular surface

Electrostatic potential (ESP) on the molecular surface is important to study the intermolecular interaction and stability of an energetic material[22]. And therefore, ESP of compound 3 (Figure 8 (a)), in which the colors range from −45 kcal mol^{-1} to 90 kcal mol^{-1} with red denoting the most negative potential and blue denoting the most positive potential, was investigated. From the figure, it can be seen that negative potentials appear to be distributed mostly on the −NO$_2$ groups, especially on the oxygen atoms while the positive potentials mainly represented on the −NH$_2$, −NH and NH$_3^+$ groups. On the other hand, the ratio of positive potentials and negative potentials were also presented (Figure 8 (b)) in order to give an intuitive view of the areas. Obviously, the ratio of the positive area (144 Å^2, 54.14%) was larger than the negative area (122 Å^2, 45.86%) which may make great contribution to the stability of compound 3 according to the stability criterion proposed by Klapotke et al.[23]

3.6 Thermal dynamic properties

Thermodynamic functions such as $C_{p,m}^0$, S_m^0 and H_m^0 were essential for further studies on other physical, chemical and energetic properties of an explosive[24]. Therefore, these data ranging from 200 to 700 K were analysed on the basis of the scaled vibrational data, principle of statistic thermodynamics and self-compiled program (Table 2). Also, the temperature-dependent relations for $C_{p,m}^0$, S_m^0 and H_m^0 in the range of 200−700 K are as follows and can be expressed as in Figure 9.

$$C_{p,m}^0 = 51.11 + 0.8318T - 0.00041T^2 \quad R^2 = 0.9999$$
$$S_m^0 = 307.13 + 1.0929T - 0.00035T^2 \quad R^2 = 0.9999$$
$$H_m^0 = -9.01 + 0.1256T - 0.00023T^2 \quad R^2 = 0.9999$$

From the data, it is obvious seen that the values of $C_{p,m}^0$, S_m^0 and H_m^0 increase as the temperature increased which may be caused by the translations and rotations of molecules at a low temperature. However, the vibrational movement is intensified at a higher temperature which in turn makes more contributions to the thermodynamic properties and lead to the increase in the thermodynamic functions. It is also found from Figure 8 that the gradients of $C_{p,m}^0$ and S_m^0 decrease while the gradients of H_m^0 increases as the temperature increases.
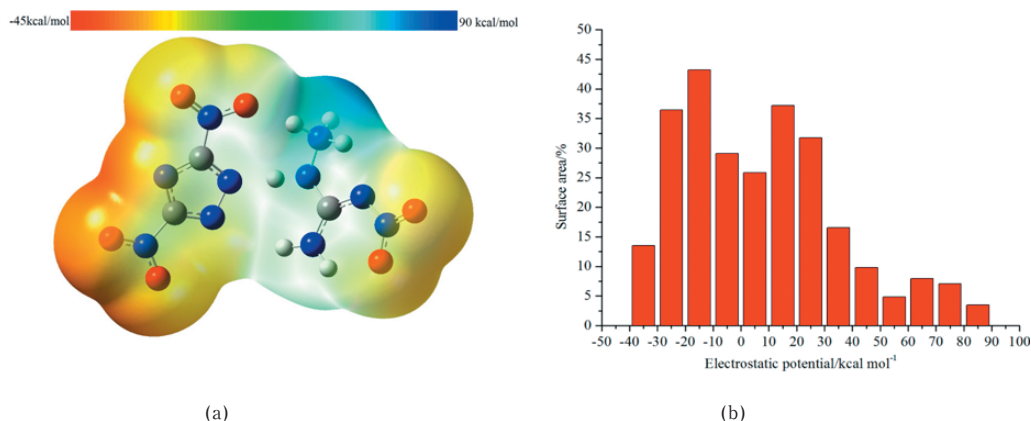
(a)   (b)

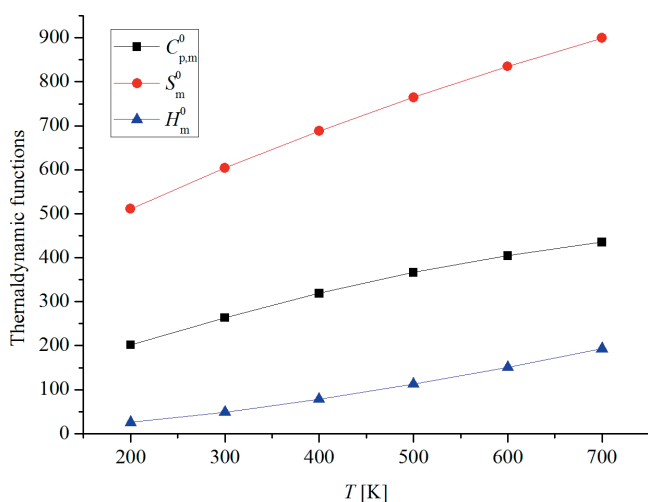**Figure 8**   ESP (a) and areas (b) of compound 3.

Figure 9   Relationships between the thermodynamic functions and temperature of compound 3.

Table 2   Thermodynamic properties of compound 3 at different temperatures.

T [K]	$C_{p,m}^0$ [J mol^{-1} K^{-1}]	S_m^0 [J mol^{-1} K^{-1}]	H_m^0 [kJ mol^{-1}]
200	201.63	510.79	25.90
300	263.61	604.46	49.20
400	319.26	688.10	78.40
500	366.35	764.57	112.74
600	404.58	834.87	151.33
700	435.23	899.63	193.36

(GPa); N, the moles of detonation gases per gram explosive; $\overline{M}$, the average molecular weight of these gases; Q, the heat of detonation (J g^{-1}), which can be calculated according to Reference 23.

Heat of formation ($\Delta H_{\text{f,salt}}$) of compound 3, which was calculated by Born-Haber energy cycle (Figure 10) and Equations (8)−(10)[26], must be known in order to obtain the heat of detonation (Q).

$$\Delta H_f^0 \text{ (ionic salt, 298K)} = \sum \Delta H_f^0 \text{ (cation, 298K)} + \sum \Delta H_f^0 \text{ (anion, 298K)} - \Delta H_L \quad (8)$$

ΔH_L, the lattice energy of the salt.

The value of ΔH_L could be predicted by the formula suggested by Jenkins et al. :

$$\Delta H_L = U_{POT} + [p \cdot (n_M/2 - 2) + q \cdot (n_X/2 - 2)] \cdot R \cdot T \quad (9)$$

U_{POT}, the lattice potential energy (Equation (10)); n_M and n_X, values that depend on the nature of the ions M^{p+} and X^{q-}, respectively.

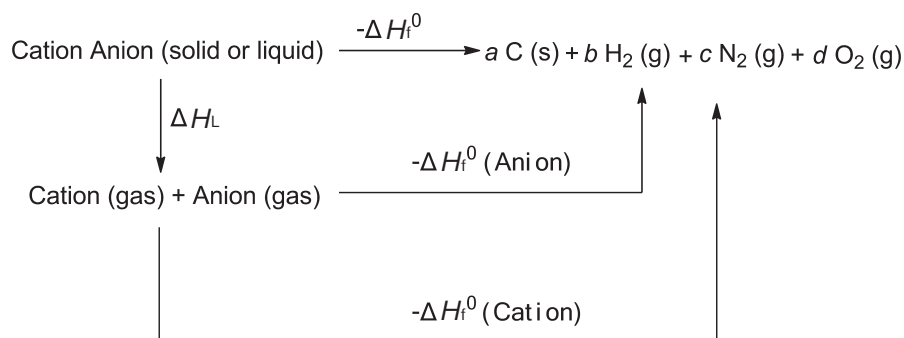$$U_{POT} = \gamma \cdot (\rho/M)^{1/3} + \delta \quad (10)$$

3.7 Energetic properties

Energetic properties such as detonation velocity (D) and detonation pressure (P) are of important parameters which can reflect the performance of an explosive. Therefore, Kamlet-Jacobs equations (Equation (6) and (7))[26] were employed to calculate the D and P of compound 3. It has been demonstrated as a reliable way to predict energetic values of an energetic material in the previous research.

$$D = 1.01 \left(N \cdot \overline{M}^{1/2} \cdot Q^{1/2} \right)^{1/2} \cdot (1 + 1.3\rho) \quad (6)$$

$$P = 1.558\rho^2 \cdot N \cdot \overline{M}^{1/2} \cdot Q^{1/2} \quad (7)$$

where ρ, the loaded density of explosives (g cm^{-3}); D, the detonation velocity (km s^{-1}); P, the detonation pressure

Figure 10   Born-Haber cycle for the formation of compound 3.

ρ, the density (1.68 g cm^{-3}), obtained by the pycnometer method ; M, chemical formula mass of the salt (g mol^{-1}) ; γ (kJ mol^{-1} cm) and δ (kJ mol^{-1}), the coefficients obtained Reference 26.

Then, energetic parameters such as ΔH_f^0 (anion, -39.1 kJ mol^{-1})[27], ΔH_f^0 (cation, 862 kJ mol^{-1})[28], ΔH_f^0 (salt, 354.7 kJ mol^{-1}), D (8.4 km s^{-1}) and P (29.8 GPa) were obtained. It is seen that compound 3 has high positive heat of formation and moderate energetic properties which meets the requirements of designing nitrogen-rich explosives and can be considered as a potential candidate of energetic material.

4. Conclusions

In summary, a new energetic material 1-amino-2-nitroguanidinium 3,5-dinitro-1,2,4-triazole salt was synthesized and characterized by IR, NMR and mass spectra. The following conclusions can be drawn : (1) thermal decomposition behavior of the title salt is a 4-stage process and the third is the most important procedure about 217.1 $^{\circ}$C with a measured decomposition enthalpy of 1252 J g^{-1} ; (2) thermal dynamic parameters such as E_k (stage 2 : 131.6 kJ mol^{-1} ; stage 3 : 139.2 kJ mol^{-1} ; stage 4 : 106.4 kJ mol^{-1}), E_o (stage 2 : 131.9 kJ mol^{-1} ; stage 3 : 139.7 kJ mol^{-1} ; stage 4 : 107.3 kJ mol^{-1}) and T_b (stage 2 : 411.1 K ; stage 3 : 456.8 K ; stage 4 : 461.8 K) were calculated ; (3) electronic properties such as charges, frontier molecular orbital and electrostatic potential show a stable structure of the title salt ; (4) detonation properties (ΔH_f^0, 354.7 kJ mol^{-1} ; D, 8.4 km s^{-1} and P 29.8 GPa) suggest that the title salt meets the requirements of designing nitrogen-rich explosives and can be considered as a potential candidate of energetic material.

Acknowledgements

References

1) P. Yin and J. M. Shreeve, Angew. Chem. Int. Edit., 54, 14513-14517 (2015).
2) T. M. Klapötke, P. C. Schmid, S. Schnell, and J. Stierstorfer, J. Mater. Chem. A, 3, 2658−2668 (2015).
3) H. Matsunaga, S. Yoshino, and M. Kumasaki, Sci. Tech. Energetic Materials, 72, 131−135 (2011).
4) M. Kumasaki, M. Nakano, and K. Sasahara, Sci. Tech. Energetic Materials, 75, 157−161 (2014).
5) Q. Yu, Z. Wang, B. Wu, H. W. Yang, X. H. Ju, C. X. Lv, and G. B. Cheng, J. Mater. Chem A, 3, 8156−8164 (2015).
6) Y. Pan, W. H. Zhu, and H. M. Xiao, J. Mol. Model., 18, 3125−3138 (2012).
7) J. Q. Yang, H. Yan, G. X. Wang, X. L. Zhang, and X. D. Gong, J. Mol. Model., 20, 2148−2160 (2014).
8) T. Wei, W. H. Zhu, J. J. Zhang, and H. M. Xiao. J. Hazard. Mater., 179, 581−590 (2010).
9) N. Fischer, T. M. Klapötke, and J. Z. Stierstorfer, Naturforsch. B, 67, 573−588 (2012).
10) X. H. Jin, B. C. Hu, and Z. L. Liu, J. Brazil. Chem. Soc., 26, 124−130 (2015).
11) N. Zohari, F. Abrishami, and M. Z. Ebrahimikia, Anorg. Allg. Chem., 642, 749−760 (2016).
12) P. Yin, C. He, and J. M. Shreeve, Chem.−Eur. J., 22, 2108−2133 (2016).
13) H. Xue, B. Twamley, and J. M. Shreeve, J. Mater. Chem., 15, 3459−3465 (2005).
14) M. J. Frisch, G. W. Trucks, H. B. Schlegel, G. E. Scuseria, M. A. Robb, J. R. Cheeseman, J. A. Montgomery, T. Vreven, K. N. Kudin, J. C. Burant, J. M. Millam, S. S. Iyengar, J. Tomasi, V. Barone, B. Mennucci, M. Cossi, G. Scalmani, N. Rega, G. A. Petersson, H. Nakatsuji, M. Hada, M. Ehara, K. Toyota, R. Fukuda, J. Hasegawa, M. Ishida, T. Nakajima, Y. Honda, O. Kitao, H. Nakai, M. Klene, X. Li, J. E. Knox, H. P. Hratchian, J. B. Cross, C. Adamo, J. Jaramillo, R. Gomperts, R. E. Stratmann, O. Yazyev, A. J. Austin, R. Cammi, C. Pomelli, J. W. Ochterski, P. Y. Ayala, K. Morokuma, G. A. Voth, P. Salvador, J. J. Dannenberg, V. G. Zakrzewski, S. Dapprich, A. D. Daniels, M. C. Strain, O. Farkas, D. K. Malick, A. D. Rabuck, K. Raghavachari, J. B. Foresman, J. V. Ortiz, Q. Cui, A. G. Baboul, S. Clifford, J. Cioslowski, B. B. Stefanov, G. Liu, A. Liashenko, P. Piskorz, I. Komaromi, R. L. Martin, D. J. Fox, T. Keith, M. A. Al−Laham, C. Y. Peng, A. Nanayakkara, M. Challacombe, P. M. W. Gill, B. Johnson, W. Chen, M. W. Wong, C. Gonzalez, and J. A. Pople, Gaussian 03, Gaussian Inc, Pittsburgh, PA, (2003).
15) X. H. Jin, B. C. Hu, Z. L. Liu, and C. X. Lv, RSC Adv., 4, 23898−23903 (2014).
16) H. E. Kissinger, Anal. Chem., 29, 1702−1706 (1957).
17) T. B. Ozawa, Chem. Soc. Jpn., 38, 1881−1886 (1965).
18) R. Z. Hu, S. L. Gao, F. Q. Zhao, Q. Z. Shi, T. L. Zhang, and J. J. Zhang, Thermal Analysis Kinetics, 2nd ed., Science Press, Beijing, (2008).
19) E. D. Glendening, C. R. Landis, and F. Weinhold, WIREs Comput. Mol. Sci., 2 1−42 (2012).
20) P. He, J. G. Zhang, K. Wang, X. Yin, X. Jin, and T. L. Zhang, Phys. Chem. Chem. Phys., 17, 5840−5848 (2015).
21) B. Kosar and C. Albayrak, Spectrochim. Acta A, 78, 160−167 (2011).
22) J. S. Murray and P. Politzer, WIREs Comput. Mol. Sci., 1, 153−163 (2011).
23) A. Hammerl, T. M. Klapotke, H. Nöth, M.Warchhold, and G. Holl, Propell. Explos. Pyrot., 28, 165−173 (2003).
24) G. Z. Zhao and M. Lu, Polycycl. Aromat. Comp., 33, 297−309 (2013).
25) M. J. Kamlet and S. T. Jacobs, J. Chem. Phys., 48, 23−25 (1968).
26) H. D. B. Jenkins, D. Tudeal, and L. Glasser, Inorg. Chem., 41, 2364−2367 (2002).
27) G. H. Tao, Y. Guo, D. A. Parrish, and J. M. Shreeve. J. Mater. Chem., 20, 2999−3005 (2010).
28) R. H. Wang, Y. Guo, Z. Zeng, and J. M. Shreeve. Chem. Commun., 19, 2697−2699 (2009).